1 **Induction of virus-induced gene silencing and *in planta* validation in cucurbits using**

2 **the CFMMV-Cm vector**

3 Sun-Ju Rhee, Yoon Jeong Jang, Jun-Young Park, Gung Pyo Lee*,[†]

4 *Department of Plant Science and Technology, Chung-Ang University, Anseong 17546, Republic*

5 *of Korea*

6 *Author for communication: gplee@cau.ac.kr

7 [†]Senior author

8 GL and SR designed the study, SR performed the experiments, analyzed the data, and drafted the

9 manuscript. YJ performed the cloning and histological analysis. JP performed the Agroinoculation

10 and phenotyping. GL supervised the data analysis, revised the manuscript, and funded the project.

11 All authors reviewed and approved the submitted version of the manuscript.

12 The author responsible for distribution of materials integral to the findings presented in this article

13 in accordance with the policy described in the Instructions for Authors

14 (https://academic.oup.com/plphys/pages/general-instructions) is Gung Pyo Lee (gplee@cau.ac.kr).

15

16 **Running title: Implementation of pCF93 for VIGS in cucurbits**

17

18 **One sentence summary**

19 The CaMV 35S promoter-driven cucumber fruit mottle mosaic virus-Cm vector (pCF93)
20 facilitates large-scale validation of male sterility-related gene functions in watermelon.
21

22 **[Email address of Author for Contact]**
23 Sun-Ju Rhee (SR): sjrhee825@gmail.com
24 Yoon Jeong Jang (YJ): jangyj770@gmail.com
25 Jun-Young Park (JP): parkjy1218@naver.com
26 Gung Pyo Lee (GL): gplee@cau.ac.kr
27
28

Abstract

Virus-induced gene silencing (VIGS) has been employed for the high-throughput analysis of endogenous gene function. We developed a CaMV 35S promoter-driven cucumber fruit mottle mosaic virus-Cm vector (pCF93) for the efficient generation of viral transcripts in plants. Using the novel pCF93 vector, we identified genes related to male sterility in watermelon (*Citrullus lanatus*), which is recalcitrant to genetic transformation. We previously reported reference-based and *de novo* transcriptomic profiling for the detection of differentially expressed genes between a male fertile line (DAH3615) and its near isogenic male sterile line (DAH3615-MS). Based on the RNA-seq results, we identified 38 *de novo*-exclusive differentially expressed genes (DEDEGs) that are potentially responsible for male sterility. Partial genes of 200~300bp were cloned into pCF93 which was then inoculated into DAH, a small type of watermelon that enables high-throughput screening with a small cultivation area. In this manner, we simultaneously characterized phenotypes associated with the 38 candidate genes in a common-sized greenhouse. Eight out of the 38 gene-silenced plants produced male sterile flowers with abnormal stamens and no pollens. Gene expression levels in flowers were validated via RT-qPCR. Stamen histological sections from male sterile floral buds and mature flowers showed developmental disruption and shrunken pollen sacs. Based on the current findings, we believe that the novel pCF93 vector and our VIGS system facilitate high-throughput analysis for the study of gene function in watermelons.

Introduction

51

52   Plant male sterility is defined by flowers producing non-viable pollen or no pollen at all, a failure

53   to dehiscent anthers, and a defective stamen. By avoiding self-pollination, male sterility

54   represents a useful tool for hybrid production, which can increase crop yield by 3.5–200% in

55   various crops (Chen and Liu, 2014; Kim and Zhang, 2018). Thus, insights obtained through

56   functional genomic studies of male sterility can present major benefits for crop breeders and

57   farmers. Within functional genomics, several techniques based on forward and reverse genetics

58   have been developed, including targeting induced local lesions in genomes (TILLING), ethyl

59   methanesulfonate (EMS) mutagenesis, and the production of the transgenic lines via T-DNA

60   tagging and RNA interference. Further, the discovery and introduction of sequence-specific

61   nucleases, such as zinc-finger nucleases (ZFNs) and transcription activator-like effector

62   nucleases (TALENs), has revolutionized gene editing (Gupta and Musunuru, 2014). However,

63   these are difficult to design and are relatively expensive. Over the past three decades, an

64   advanced gene editing technology named 'CRISPR/Cas9' system has been developed and

65   introduced for use in humans, animals, as well as plants (Pickar-Oliver and Gersbach, 2019).

66   Although the CRISPR/Cas9 system is a promising tool, it generally requires the generation of

67   transgenic plants via Agrobacterium-mediated or protoplast transformation (Fister et al., 2018;

68   Shan et al., 2020). This bottleneck has been addressed to enable the application of CRISPR/Cas9

69   in various plants that are recalcitrant to genetic modification. In general, cucurbit plants have

70   extremely low efficiency of transformation. To date, several studies have reported the generation

71   of cucurbit knock-out mutants by using CRISPR/Cas9 (Hu et al., 2017; Tian et al., 2017; Tian et

72   al., 2018). However, the requirement for a stable genetic transformation technique, which is not

73   as laborious and time-consuming, remains.

74   The virus-induced gene silencing (VIGS) system represents one such alternative as it enables fast

75   and straightforward high-throughput gene screening for functional genomics. Improved VIGS

76   vectors are very recently reported. The Maize dwarf mosaic virus vector could targeted multi

77   endogenous gene simultaneously (Xie et al., 2021) and the Pr CMV-LIC VIGS vector adopted

78   ligation-independent cloning (LIC) strategy for high-throughput cloning (Li et al., 2021). The

79   modified TRV vector is developed for efficient validation system through marker pds gene in

80   front of the multiple cloning site (MCS) (Yamamoto et al., 2021). Efficient and easy-to-handle

81   VIGS systems are in the spotlight for high-throughput screening of the gene functions.

82   VIGS is based on post-transcriptional gene silencing (PTGS), which is a defense mechanism of

83   host cells against viral infection (Robertson, 2004). During plant infection, viral dsRNA is

84   formed through replication. These dsRNAs are degraded by DCL2/DCL4, resulting in the

85   generation of siRNAs. The siRNAs are in turn recruited to endogenous mRNA or viral RNA via

86   the RISC complex based on sequence homology. The targeted mRNA and viral RNA are

87   degraded as a consequence. In order to utilize PTGS in functional genomics, plant virus vectors

88   have been extensively developed in order to apply VIGS systems in various plant species, such

89   as tomato (Liu et al., 2002; Fu et al., 2005; Senthil-Kumar and Mysore, 2011; Rhee et al., 2018),

90   Chinese cabbage (Yu et al., 2019), rice (Purkayastha et al., 2010; Kant et al., 2015), maize

91   (Benavente et al., 2012; Mei et al., 2016), barley (Liu et al., 2016), strawberry (Li et al., 2019),

92   and, more recently, cucurbits (Igarashi et al., 2009; Bu et al., 2019; Liao et al., 2019) as well as

93   banana (Tzean et al., 2019).

94   We previously constructed a virus vector for functional genomic studies in cucurbits, particularly

95   of their flowers and fruits, using *Cucumber fruit mottle mosaic virus* (CFMMV). CFMMV is a

96   member of the *Tobamovirus* genus and has a monopartite genome of 6.5 kb that is comprised of

4

97   four ORFs, which encode 127-kDa and 187-kDa proteins involved in virus replication as RNA-

98   dependent RNA polymerases (RdRps), a 30-kDa movement protein (MP) required for cell-to-

99   cell movement of the virus, and a 17-kDa coat protein (CP) that is essential for long-distance

100   movement (Antignus et al., 2001). CFMMV infects a wide range of cucurbits encompassing

101   major commercial crops such as cucumber (*Cucumis sativus)*, melon (*Cucumus melo*), squash

102   (*Cucurbita pepo*), and watermelon. Our groups previously isolated and sequenced CFMMV-Cm

103   from melon to construct a full-length infectious clone (Rhee et al., 2014). We further confirmed

104   that viral *in vitro* transcripts stably replicate in cucurbit fruits. Subsequently, we mapped the sub-

105   genomic protein (SGP) of CP and constructed a CFMMV vector, which successfully expressed

106   EGFP in cucumber, melon, and watermelon (Rhee et al., 2016).

107   The functional genomics analysis of watermelon has been challenging because of the recalcitrant

108   nature of the species with regard to the generation of transgenic plants. Further, the study of

109   watermelon fruit development demands a relatively long time as well as large areas for

110   cultivation.

111   In this study, we report an efficient cucurbit-infecting virus vector system based on the CFMMV

112   VIGS vector, which exhibited high and long-lasting gene silencing efficiency in cucurbit plants,

113   with clear phenotypes. Our monopartite CFMMV vector is relatively easy to manipulate and

114   allows the high-throughput screening of gene function in watermelon. This CFMMV VIGS

115   system will help advance the study of gene function in cucurbit reproductive organ development.

116

117

118

Results

Constructing an efficient CFMMV vector for VIGS

In order to determine the most efficient VIGS vector, four CFMMV-Cm-based vectors (pCF93, pCF93K, pCF157, and pCF157K) were assessed based on our previous report (Rhee et al., 2016). pCF93 and pCF157 have one 3'NTR, while pCF93 and pCF157 have an additional 3'NTR between the MCS and CP region (Figure 1A). To visualize the gene silencing efficiency of CFMMV-Cm-based vectors, the partial *phytoene desaturase* (*pds*) gene was inserted into each vector. Infection symptoms were observed at 5-6 dpi on the second upper leaf of inoculated leaves, and a photo-bleached phenotype developed at 12-15 dpi (Figure 1B, 1C). The typical photo-bleached phenotype was not observed in *Nicotiana benthamiana* infected with pCF157K-nbpds (Figure 1C). Comparison of the gene silencing phenotypes between pCF93-nbpds and pCF157-nbpds revealed that plants infected with the former had wider white-leaf areas than those of infected with pCF157-nbpds. When the CFMMV-Cm-based vector carrying *PDS* was inoculated into *N. benthamiana*, virus symptoms appeared at 5-6 dpi on the second upper leaf from the inoculated leaves, and photo-bleached phenotypes developed at 12-15 dpi. In *N. benthamiana* infected with pCF157K-nbpds, systemic viral symptoms were observed, while photo-bleached phenotypes did not develop. To confirm the inserted gene stability of the vector, quantitative reverse transcription PCR (RT-qPCR) was conducted using det-F and det-R primers designed based on the flanking regions nearby the MCS. After inoculation with pCF93, pCF93K, and pCF157 carrying nbpds, total RNA was isolated from fourth upper leaves above the inoculated leaves in order to confirm their genomic composition via RT-qPCR. Products of expected size were obtained (blue arrow in Supplemental Figure S2). However, pCF157K-nbpds lost the artificially inserted MCS region and returned to the genome structure of wild-type

142   CFMMV via homologous recombination (Supplemental Figure S2). Although pCF93K-nbpds

143   induced photo-bleaching phenotypes, it exhibited low gene silencing efficiency as compared to

144   pCF93-nbpds and pCF157-nbpds. Thus, the vectors without an additional 3'NTR were better

145   suited for VIGS. We selected pCF93 as the most efficient VIGS vector for gene function
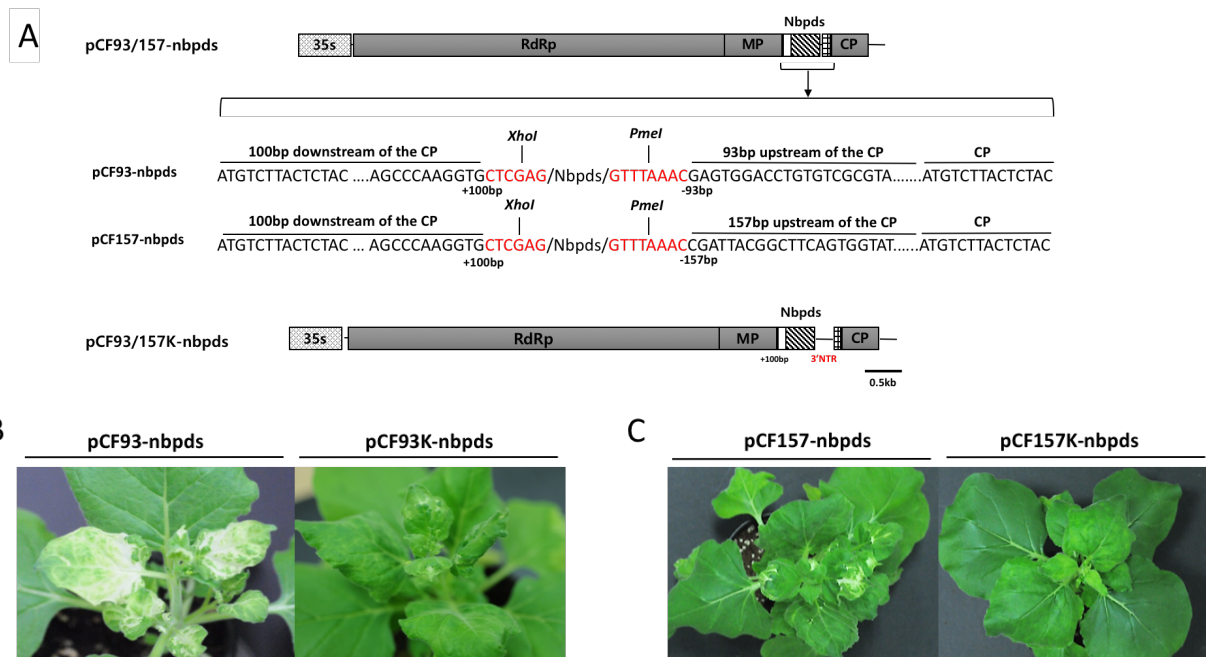
146   analysis.

147

148

149
150

Figure 1. Virus-induced gene silencing of the *PDS* gene resulting in a photobleaching phenotype in *N. benthamiana.* Schematic diagrams of pCF93/157-nbpds and the nucleotide sequence around the MCS region. *Xho*I and *Pme*I are restriction enzyme site for insert cloning. *35S*, Cauliflower mosaic virus 35S promoter; *5' NTR*, 5' non translated region; *RdRp*, RNA-dependent RNA polymerase; *MP*, triple gene block; *CP*, coat protein; *3'NTR;* 3' non translated region (A), comparison of VIGS phenotypes in *N. benthamiana* infected by pCF93-nbpds and pCF93K-nbpds (B) as well as pCF157-nbpds and pCF157K-nbpds (C) at 12 days post-inoculation (dpi). Of the four constructs tested, pCF93 exhibited the most efficient silencing. Thus, we selected pCF93 for VIGS.

Evaluation of pCF93 as a VIGS vector in cucurbits

PDS-carrying pCF93 was inoculated into cotyledons of cucumber, melon, and watermelon in order to validate VIGS efficiency in cucurbits. *N. benthamiana* has been used to evaluate the

8

164   gene silencing efficiency of various VIGS vectors (Rhee et al., 2016). The *PDS* expression levels

165   of *N. benthamiana* infected with pCF93-nbpds exhibited a 5-fold reduction (Figure 2A). Melon

166   infected with pCF93-cmpds exhibited photobleaching phenotypes in the middle areas of the

167   plant, including the stems and leaves, maintaining these phenotypes in the newly developed

168   leaves until its death (Figure 2B). Likewise, the leaves of watermelon exhibited photobleaching

169   phenotypes and a *PDS* mRNA level reduction of up to 333-fold when compared to p35SCF-

170   Cm_{flc}-infected counterparts (Figure 2C). The cucumber also exhibited *PDS*-silenced phenotypes

171   in the leaves and flowers. The *pds* mRNA level in the leaves of pCF93-cspds-infected cucumbers

172   was reduced about 7-fold relative to that in p35SCF-Cm_{flc}-infected cucumbers. Flowers also

173   exhibited gene silencing phenotypes and an approximately 2.5-fold reduction in *PDS* mRNA

174   expression under pCF93-cspds infection relative to that under p35SCF-Cm_{flc} infection, as

175   determined via RT-PCR (Figure 2D). Of note, all plants infected with the tested virus vectors

176   were transferred from the growth room to a greenhouse under the sunlight in order to enhance
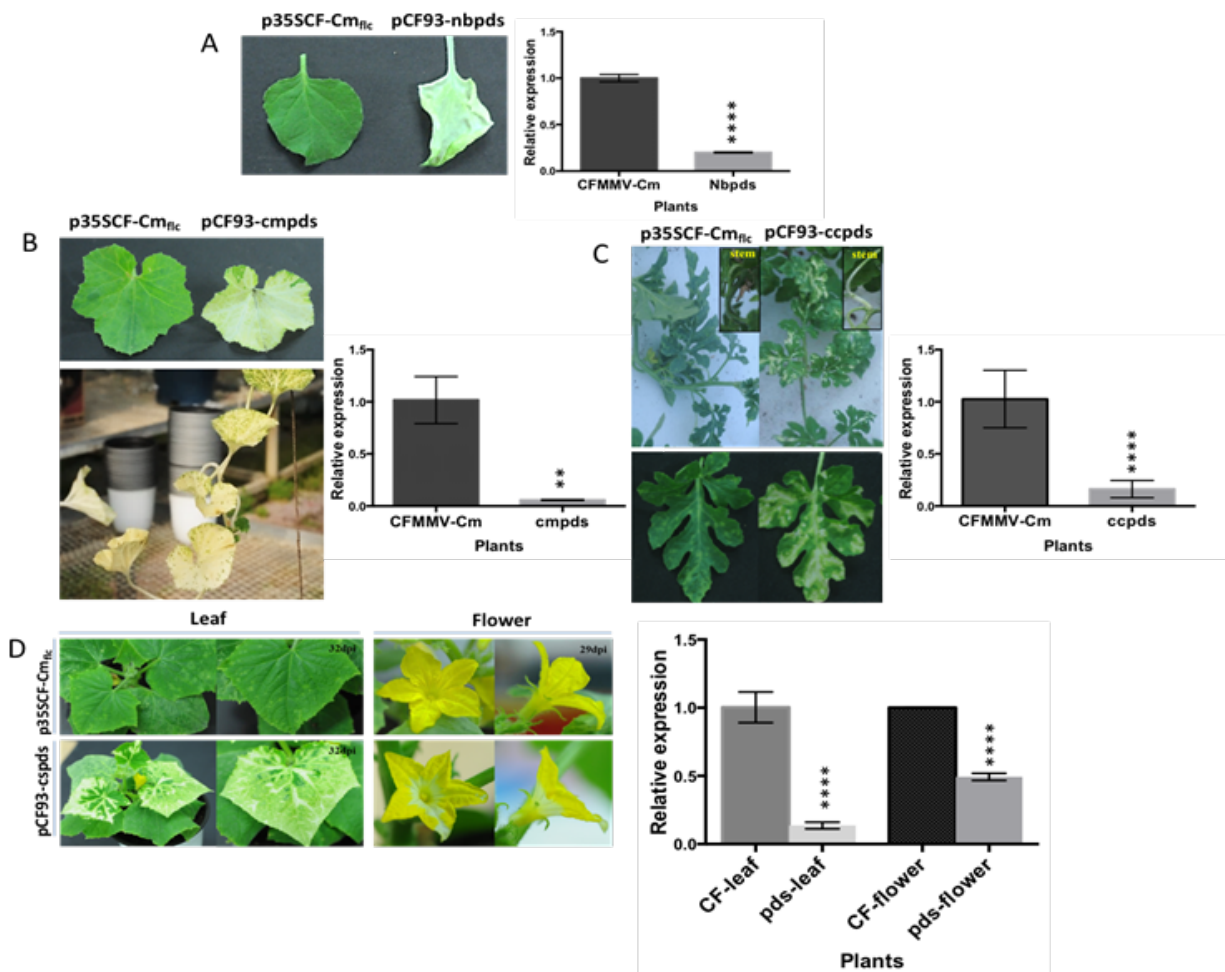
177   *PDS* VIGS efficiency.

178

Figure 2. The effects of virus-induced *PDS* silencing on phenotype in various plants. (A) Photobleaching phenotypes and relative expression levels of endogenous *PDS* mRNA in *N. benthamiana* leaves infected with pCF93-nbpds. (B) Comparison of gene silencing efficiency in melon leaves infected with p35SCF-Cm_{flc} (top, left) and pCF93-cmpds (top, right). pCF93-cmpds-induced VIGS phenotypes in melon grown in greenhouse (Bottom). (C) Photobleaching phenotypes on watermelon leaves and stem infected with pCF93-ccpds. Relative expression levels of *PDS* after silencing via pCF93-ccpds compared to those in watermelon infected with wild-type CFMMV, as determined via real-time qPCR. (D) Photobleaching of cucumber leaves and flowers infected with pCF93-cspds. *PDS* mRNA levels in cucumber leaves and flowers infected with p35SCF-Cm_{flc} (denoted as CF-leaf and CF-flower, respectively) and pCF93-cspds

10

190 (denoted as pds-leaf and pds-flower, respectively). Relative *pds* expression was determined using

191 *PDS*-specific primers and normalized to GAPDH expression. (A) 18S rRNA expression level (B,

192 C, and D). Relative expression levels were determined by setting arbitrary value (1.0) to the

193 expression level of CFMMV-Cm, which used as a calibrator sample. Statistical analysis was

194 performed using the Student's t-test (****p < 0.0001 and 0.001<**p< 0.01).

195

196 **Evaluation of *PDS* gene silencing efficiency in three watermelon cultigens**

197 Flowers and fruits are the major reproductive organs giving rise to edible parts of plants,

198 especially cucurbits. Therefore, many researchers have studied the functional genomics of

199 cucurbit fruit and flower development (Lin et al., 2007; Wang et al., 2010; Manzano et al., 2014;

200 Switzenberg et al., 2015). *pds* carrying pCF93 was Agro-inoculated to the cotyledons of

201 watermelon, and the plants were grown in greenhouse conditions without any additional

202 infections. Three cultigens of watermelon, namely '2401', 'Chris cross', and 'DAH' (a small-

203 fruit type of watermelon), were used for evaluating pCF93-ccpds VIGS efficiency. Watermelon

204 fruits were harvested at 45 days after pollination (dap) and exhibited photobleaching phenotypes

205 on the peels (Figure 3A). When the watermelon plants were infected with pCF93-ccpds, the fruit

206 peels and flesh turned white. As the red flesh of watermelon is packed with lycopene and β-

207 carotene (Tomes et al., 1963), we presumed that the color change to white was caused by photo-

208 bleaching, which is responsible for the degradation of chlorophyll. White-colored flesh can also

209 develop as a result of the inhibition of lycopene and β-carotene biosynthesis. Thus, lycopene and

210 β-carotene content were estimated via HPLC analysis, and *PDS* expression was determined via

211 semi-RT-qPCR. The lycopene and β-carotene contents of the fruits (45 dap) decreased

212 significantly in all three watermelon cultigens. The flesh color of all tested watermelon fruits

213   became white, which was attributed to the blockade of lycopene synthesis. The lycopene and β-

214   carotene contents of pCF93-ccpds-infected watermelon decreased approximately 3- to 110-fold

215   and 2.7- to 21-fold, respectively, as compared to those in p35SCF-Cm$_{flc}$-infected fruit (Figure

216   3B, C, and D). *PDS* gene expression was suppressed in all watermelons subjected to *PDS*

217   silencing (Figure 3E). Chlorophyll a content in the peels of pCF93-ccpds-infected watermelons

218   was reduced about 2.5- to 15-fold compared to that of p35SCF-Cm$_{flc}$-infected plants, while

219   chlorophyll b content exhibited a 1.4- to 8-fold reduction. Total chlorophyll was reduced about

220   1.13- to 2.5-fold (Figure 3F and G). Of note, lycopene and β-carotene content were successfully

221   repressed in the fruits of all three watermelon cultigens.
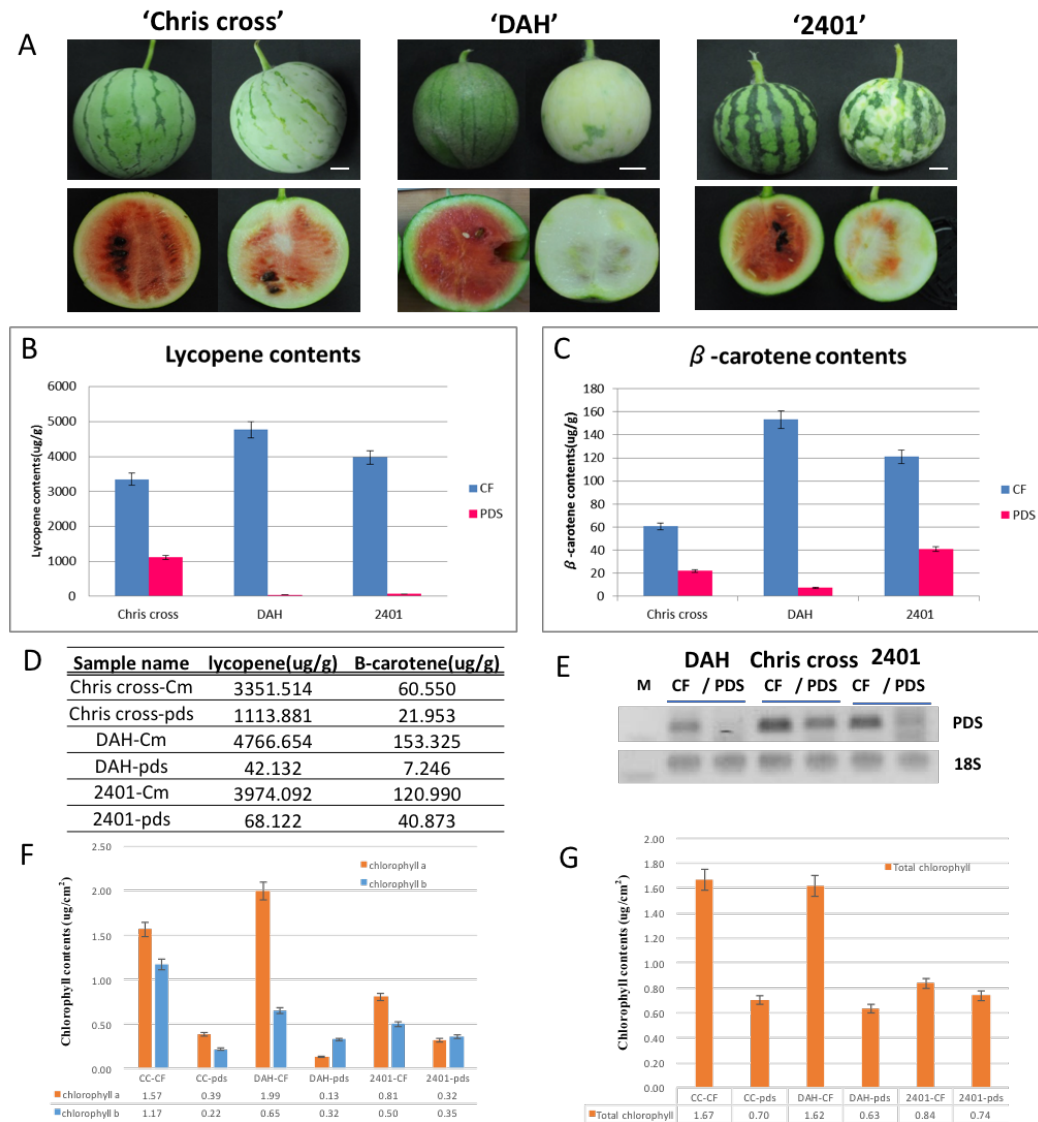
222

Figure 3. Estimation of lycopene and β-carotene contents in watermelon fruits ('Chris cross', 'DAH', and '2401') and semi-quantitative RT-qPCR for the detection of endogenous phytoene desaturase (PDS) expression. VIGS phenotypes in the fruits of three cultigens of watermelon. Scale bars=2 cm (A). Quantification of lycopene (B) and β-carotene (C) contents in flesh of watermelon fruits infected with p35SCF-Cm$_{flc}$ (blue bar, indicated as 'CF') and pCF93-ccpds (pink bar, indicated as 'PDS'). Lycopene and β-carotene contents were determined via HPLC. Lycopene and β-carotene contents presented in a table (D), semi-quantitative RT-qPCR

13

232   was performed using a ccpds-specific primer set (E). Estimation of Chlorophyll a and b contents

233   in peels of watermelon infected by CFMMV vector (F), Calculated total chlorophyll contents

234   (G). Watermelon cultigens 'Chris cross', 'DAH' and '2401' infected by p35SCF-Cm$_{flc}$ are

235   denoted as 'CC-CF', 'DAH-CF' and '2401-CF', respectively. 'Chris cross', 'DAH' and '2401'

236   infected by pCF93-ccpds are denoted as 'CC-pds', 'DAH-pds' and '2401-pds', respectively.

237

238   **Verification of candidate genes related to male sterility in watermelon by using the**

239   **CFMMV-VIGS system**

240   We previously conducted reference- and *de novo* RNA-seq to detect differentially expressed

241   genes (DEGs) between the MS and MF lines of DAH3615 (Rhee et al., 2015; Rhee et al., 2017).

242   We identified a total of 38 *de novo*-exclusive DEGs (DEDEGs) and inserted partial genes into

243   pCF93 vectors for gene function analysis (Supplemental Table S1). Watermelon plants infected

244   with vectors for the silencing of each DEG were simultaneously cultured in the greenhouse and

245   studied.

246   Silencing eight of the DEDEGs, which included calcium-dependent protein kinase 2 (*CDPK2*),

247   elongation factor 1-alpha (*EF1a*), late embryogenesis abundant protein 1 (*LEA1*), LIM domain

248   protein (*LIM*), mitotic spindle assembly checkpoint protein MAD2 (*MAD2*), polygalacturonase

249   (PG), fasciclin-like arabinogalactan protein 5 (*FLA5*), and expansin-A9 (*EXPA9*), resulted in

250   typical male sterility phenotypes (Table 1).

251

252

253

254 **Table 1.** Eight out of the 38 putative genes from reference-based and *de novo* transcriptome data,

255 which were silenced in watermelons via VIGS.

Gene symbol	Research	Uniprot_ID	Gene_ID	Annotation
V4	Reference-based	Q3YAT0_PETIN	Cla010883	Calcium-dependent protein kinase 2
V8	Reference-based	B9SPV9_RICCO	Cla000553	Elongation factor 1-alpha
V9	Reference-based	LEA1_CICAR	Cla007634	Late embryogenesis abundant protein 1
V10	Reference-based	Q306K1_BRANA	Cla001608	LIM domain protein
V12	Reference-based	D2V3A0_NAEGR	Cla009991	Mitotic spindle assembly checkpoint protein MAD2
V15	Reference-based	E3VSV7_CUCPE	Cla016924	Polygalacturonase
V24	De novo	FLA5_ARATH	c9925_g1	Fasciclin-like arabinogalactan protein 5
V28	De novo	EXPA9_ARATH	c29764_g1	Expansin-A9

256

257 The coding sequence (CDS) information was obtained from the watermelon genome database of

258 the Cucurbit Genomics Database (http://cucurbitgenomics.org/), and candidate gene primers

259 were designed to detect the insertion of pCF93 (Table S2). All DAH plants infected with the

260 eight constructs produced complete or partially abnormal MS flowers in the same plant (Fig. S3
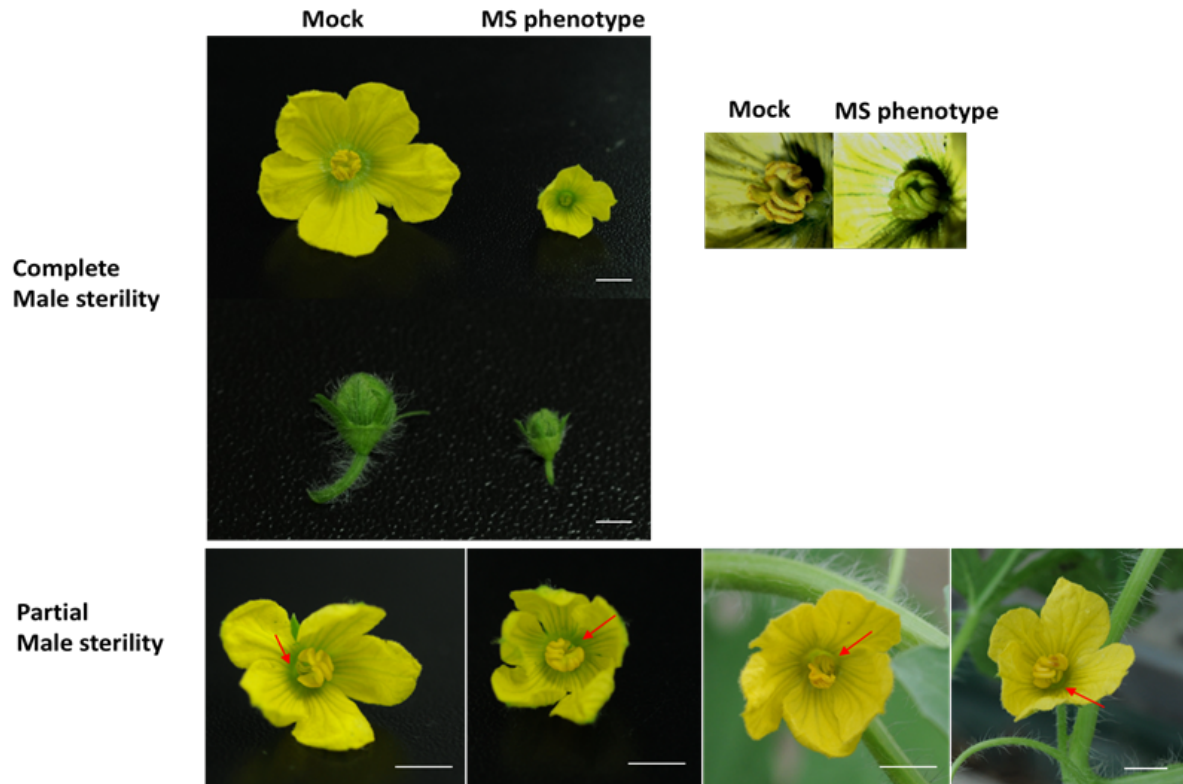
261 and Fig. 4).

262

263

15

264
265 **Figure 4. Male sterile flowers developed in candidate gene-silenced watermelon.** Complete

266 male sterility observed in candidate gene-silenced plants. Some of the flowers exhibited partial

267 male sterility. Representative flowers in the top panel were collected from pCF93-pds-int

268 (denoted as 'mock') and EXPA9-silenced plants (denoted as 'MS phenotype'). Partially

269 abnormal male sterility flowers developed in LIM-, MAD2-, FAP5, and PG-silenced plants

270 (from left to right, respectively). Red arrows indicate the aborted stamen. Scale bars=0.5 cm.

271
272 The wild-type watermelon male flower consists of three individual stamens. The complete MS

273 flower exhibited an almost 3-fold size reduction as well as small green immature stamens and no

274 pollens. The partially abnormal MS flower showed developmental disruption of one or two

275 stamens as well as no pollens. However, the normally developed stamens of partially abnormal

276 MS flowers produced pollens. The *LEA1*-silenced plant produced complete MS flowers but no

277 partially abnormal MS flowers. The seven remaining gene-silenced plants produced both

16

278   complete and partially abnormal MS flowers. The phenotypes of all virus-induced MS flowers

279   appeared similar to each other as well as to the male sterile line 'DAH3615-MS'. To characterize

280   anatomical differences between MS and MF stamens, histological cross-sections were evaluated.

281   MF floral buds and flowers were collected from mock-inoculated plants infected with pCF93-

282   pds-int. DAH3615-MS did not produce pollen grains, and stamens appeared immature based on

283   visual examination. MF floral buds and flowers produced normal pollen sacs and pollen, whereas

284   MS showed developmental disruption of tapetum cells and microspore mother cells. The mature

285   flowers had atrophied pollen sacs that consisted of abnormal shrunken cells (Figure 5, indicated

286   by red arrow). RT-qPCR was then performed to determine the expression of the eight DEDEGs

287   and explore their interaction. We collected three mature flowers showing a complete MS

288   phenotype and pooled their total RNA. Most of the genes exhibited a tendency toward

289   suppression in virus-infected MS flowers (Figure 6). The *LEA1*-silenced flowers exhibited

290   dramatic induction of the *LIM* gene, approximately 290-fold compared to that of pds.int-infected

291   plants. Conversely, the *LIM*-silenced flowers exhibited reduced *LEA1* expression. *EXPA9*

292   expression was induced via *FLA5* downregulation, while *CDPK2*, *MAD2*, *PG*, and *FLA5* were

293   suppressed in all flowers showing the MS phenotype. Notably, all MS phenotype flowers

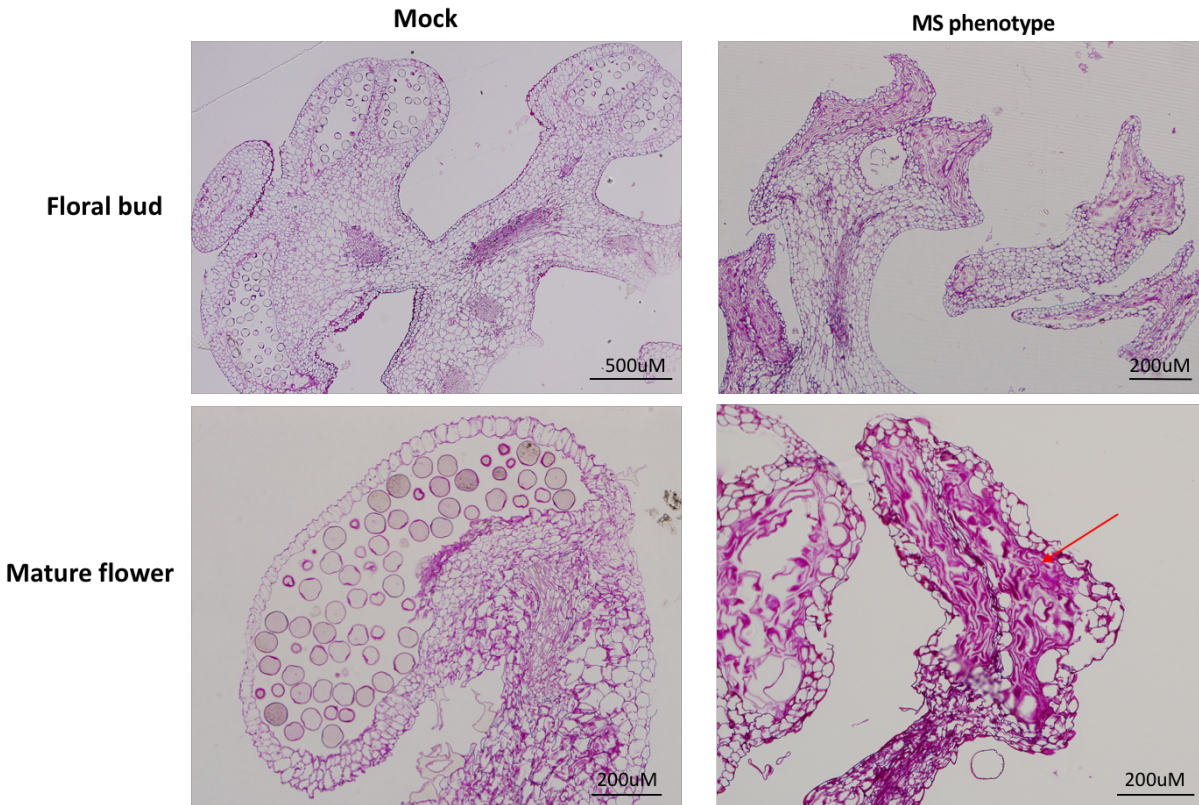294   exhibited extreme reduction in *MAD2* expression.

295

17

Figure 5. Histological sections of stamens from floral buds and mature flowers of mock-inoculated and candidate gene-silenced plants. The floral buds of plants infected with pCF93-pds-int (denoted as 'mock') formed normal pollen sacs containing pollen grains. In contrast, floral buds of candidate gene-silenced plant showed an absence of pollen. Pollen sacs of mature flowers exhibited normal morphology in mock flowers, but those of candidate gene-silenced plants were atrophied (red arrow). MS flower collected from an EXPA9-silenced plant (denoted as 'MS phenotype'). Scale bars are 200 μm and 500 μm.
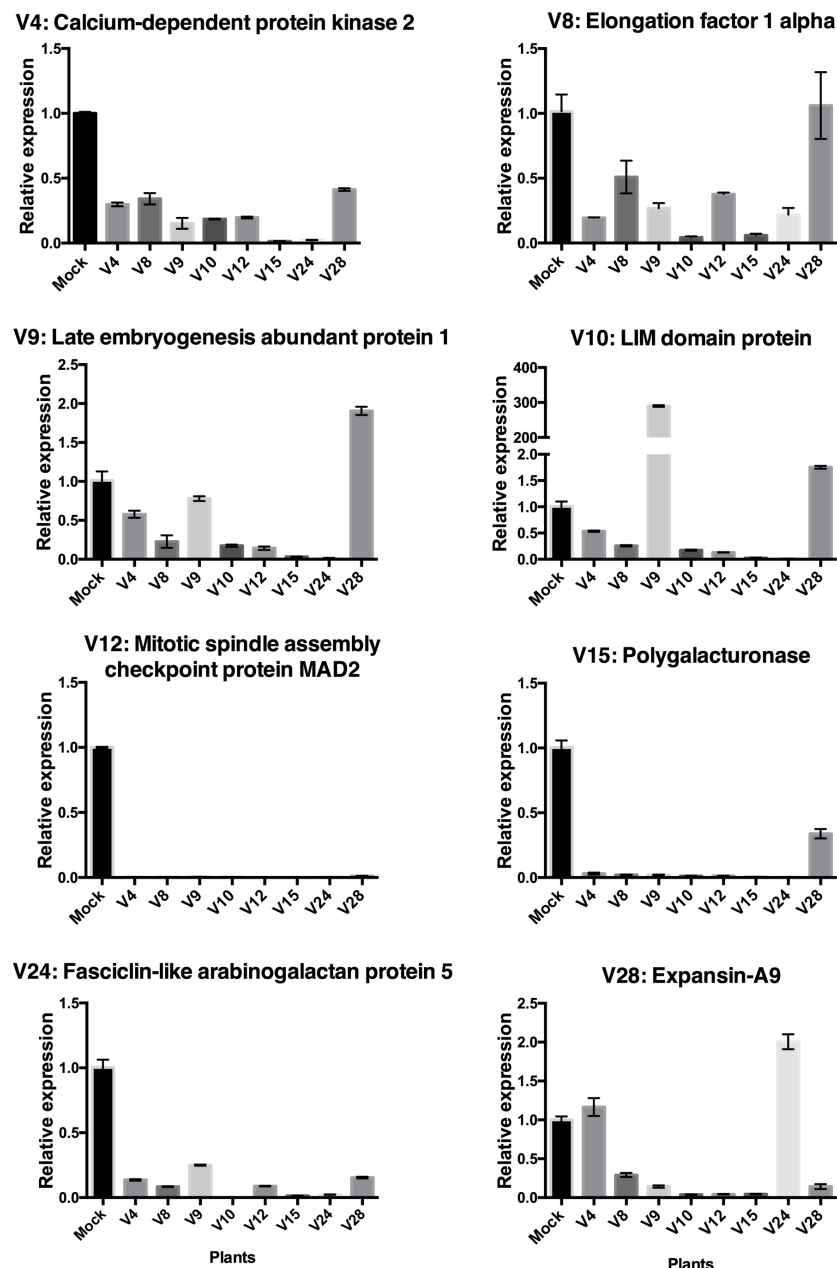
306
307

Figure 6. Male sterility-related candidate gene expression. Transcript levels were analyzed

via RT-qPCR. Relative expression was normalized to 18S rRNA as a housekeeping gene. The

transcript levels of eight candidate genes (Calcium-dependent protein kinase 2, Elongation factor

1 alpha, Late embryogenesis abundant protein 1, LIM domain protein, Mitotic spindle assembly

checkpoint protein MAD2, Polygalacturonase, Fasciclin-like arabinogalactan protein 5, and

313   Expansin-A9) were analyzed in all construct-infected plants. Each graph presents the relative

314   expression of a candidate gene in the gene-silenced plants (x-axis). Relative expression levels

315   were calculated by setting the expression level of pCF93-pds-int (denoted as 'mock') to 1.0 in

316   arbitrary units (y-axis). Statistical analysis was performed using one-way ANOVA, followed by

317   Tukey's post hoc test for multiple comparisons.

318

319   Discussion

320   Due to limitations associated with the genetic editing of cucurbits, genomic research into these

321   species has been slower when compared to other plants. To address this issue, we previously

322   isolated and constructed a CFMMV-Cm-based full-length clone (Rhee et al., 2014) and a virus

323   vector for heterologous expression (Rhee et al., 2016). Fourteen CFMMV vectors were

324   developed, carrying -55, -77, -81, -93, -100, -110, -121, -127, -148, -152, -157, -170, -180, and -

325   187bp upstream positions from the CP start codon to the +100bp SGP, respectively. In previous

326   studies on *Tobacco mosaic virus* (TMV), viral gene expression was reported to depend on the

327   proximity of the ORF to the 3' terminus (Culver et al., 1993). When the MP gene was located

328   before the 3' terminus, expression increased up to 20 times relative to that of the wild-type virus

329   (Culver et al., 1993). The insertion of an additional 3'NTR between two coat proteins led to

330   similar expression levels (Lindbo, 2007). Thus, it was suggested that proximity to the 3'NTR is a

331   crucial factor for enhancing expression. TMV vectors were also designed with duplication of the

332   TMV 3' NTR between the foreign ORF and CP gene (Shivprasad et al., 1999). Based on these

333   previous findings, two types of virus vectors were developed herein, one possessing a 3'NTR

334   and the other possessing tandemly duplicated 3'NTRs, named CFMMV and CFMMV-K,

335   respectively.

336   Among the previously developed vectors, -93 and -157 exhibited high EGFP expression

337   efficiency. Therefore, pCF93, pCF93K, pCF157, and pCF157K were inoculated to evaluate

338   VIGS efficiency in the current work. *N. benthamiana* infected with pCF93-nbpds, pCF93K-

339   nbpds, and pCF157-nbpds developed photobleaching phenotypes, while gene silencing was

340   unsuccessful in the pCF157K-nbpds-infected plant (Figure 1). pCF93K-nbpds and pCF157K-

341   nbpds inserts were easily lost due to homologous recombination. *N. benthamiana* infected with

342   pCF93-nbpds exhibited 5-fold lower levels of *PDS* mRNA in the leaves relative to pCF157-

343   nbpds-infected plants.

344   pCF93-pds successfully induced gene silencing not only in leaves but also in the reproductive

345   organs of cucurbits, including melon, cucumber, and watermelon. PDS is involved in the β-

346   carotene biosynthesis pathway which is implicated in the color of flowers. Moreover, *PDS*

347   downregulation can lead to inhibition of lycopene and β-carotene biosynthesis, resulting in the

348   color change of watermelon flesh to white.

349   VIGS is sensitive to the genotypes of specific plant species (Bekele et al., 2019). Thus, three

350   types of watermelon cultigens were evaluated in the current work. All cultigens exhibited gene

351   silencing phenotypes, with fruits developing white-colored peels due to chlorophyll degradation

352   and a reduction of lycopene content. Among evaluated cultigens, the DAH line showed the most

353   pronounced silencing phenotypes and was selected for subsequent experiments. All three

354   cultigens were small and could be grown in 16-cm pots with stable fruit development and

355   ripening. Thus, our research required a relatively small cultivation area relative to common

356   watermelon cultivation. Taken together, the VIGS approach described herein allows for

357   convenient and relatively effortless watermelon research.

21

358   To functionally validate the 38 DEDEGs we identified, we inserted partial genes into the pCF93

359   vector which was then inoculated into DAH-MF seedlings via agroinoculation. Approximately

360   400 plants were inoculated and grown at once in the greenhouse (Supplemental Figure S1).

361   Silencing eight of the 38 candidate genes seemed to induce male sterility, yielding different male

362   sterile flowers within a single plant. To identify crucial genes implicated in male sterility, we

363   evaluated the expression of these eight genes in MS flower samples. All genes exhibited a

364   tendency toward downregulation in MS flowers, but no significant differences were observed in

365   *EF1a*, *LEA1*, *LIM*, and *EXPA9* expression relative to mock-infected plants. EF1a is essential for

366   translation, particularly elongation, and exhibits ubiquitous expression, which includes the

367   reproductive organs of plants (Cosgrove et al., 1997; Wang et al., 2004). Thus, the

368   downregulation of EF1a might affect male sterility-related gene expression. LIM, LEA, and

369   Expansin play an important role in pollen formation and pollen tube elongation (Ye and Xu,

370   2012). Thus, we suspected that these four genes affect male sterility but might not be directly

371   involved in the mechanism underlying MS. Of note, *CDPK2*, *FLA5*, *PG*, and *MAD2* were

372   downregulated in all gene-silenced samples. There are several reports suggesting that CDPKs are

373   involved in the regulation of pollen tube growth (Myers et al., 2009; Li et al., 2018). Thus, we

374   suspect that CDPK2 downregulation might be indicated by the absence of pollen grain. PG is a

375   representative hydrolytic enzyme involved in various functions such as plant cell wall

376   deposition, fruit ripening, abscission, pollen intine and exine formation, as well as pollen tube

377   growth via pectin rearrangement (Kulikauskas and McCormick, 1997; Huang et al., 2008; Jiang

378   et al., 2014; Lyu et al., 2015). As our virus-infected MS flower did not produce pollen grain and

379   exhibited an immature stamen, PG deficiency might have compromised stamen formation and

380   pollen production. FLAs are subclass of arabinogalactan proteins (AGPs), which have

381   pleiotropic functions implicated in plant reproduction and pollen development (Pennell and

382   Roberts, 1990; Coimbra et al., 2007). AtFLA3 (*Arabidopsis thaliana FLA3*) knock-down plants

383   produced abnormal pollens, and an overexpression line exhibited defective stamen filaments (Li

384   et al., 2010). It was therefore, suggested that FLA3 participates in microspore and reproductive

385   organ development.

386   Remarkably, *MAD2* expression was not detected in all virus-induced MS flowers (Figure 6).

387   MAD2 is essential for chromosome segregation during mitosis, controlling the metaphase-to-

388   anaphase transition (Shah and Cleveland, 2000). SAC is known as a crucial regulator for genome

389   stability in humans, animals, and yeast (Lara-Gonzalez et al., 2012). While the functional

390   significance of plant *MAD2* is still unclear, equal segregation of chromosomes is definitely

391   essential for normal development. Arabidopsis and maize MAD2 homologues localized at the

392   kinetochore, and maize MAD2 was reported to be sensitive to microtubule attachment during

393   meiosis and mitosis (Yu et al., 1999). While the Arabidopsis MAD2-2 mutant did not affect

394   reproductive organ development, it did compromise root growth. Lack of BUB1, which is one of

395   the SAC components along with MAD2, induced male sterility in rice (Burgos-Rivera and

396   Dawe, 2012). Taken together, the suppression of mitosis-related genes can give rise to male

397   sterility in plants.

398   In the present study, we established a high-throughput screening system for the identification of

399   putative male sterility-related genes deduced from massive RNA-seq data. This approach

400   facilitated the functional genomic study of watermelon, which normally requires huge cultivation

401   area in a short time for the simultaneous study of many genes of interest, in a common-sized

402   greenhouse (Supplemental Figure S1). The use of small-fruit type watermelons planted in pots is,

23

403   therefore, essential for reducing the study area, and it may also lower the risk of soil

404   contamination.

405   The current work adds to the body of evidence regarding the major advantage of the VIGS

406   system. The, pCF93 vector established silencing in the various organs throughout the lifetime of

407   the plant. Taken together, pCF93 is a very useful tool for high-throughput screening and is

408   particularly advantageous in fruit development.

409   To our knowledge, this is the first report on the application of VIGS for evaluating endogenous

410   gene function in watermelon fruits, highlighting the utility of pCF93 in cucurbits. The current

411   work establishes a theoretical and practical basis for future studies focused on functional

412   genomics analysis in cucurbits.

413

Materials and methods

415   **Plant materials**

416   We used *Nicotiana benthamiana, Cucumis sativus* L. 'Porisian pickling', *Cucumis melo* L.

417   'Early hanover', as well as *Citrullus lanatus* L. 'Chris cross', '2401', and 'DAH' for VIGS. The

418   cultigens   were obtained from the gene bank of the National Agrobiodiversity Center (NAC),

419   Rural Development Administration (RDA), Jeonju, South Korea. The plants were grown under a

420   constant temperature of 28℃ with a 16/8-h light/dark cycle. Cucumber, melon, and watermelon

421   plants were transferred to greenhouse 2~3 weeks after inoculation. Each shelf in the green house

422   is 150 × 270 cm and has 28 pots. For one experimental set of MS VIGS, we performed 14

423   replicates per putative gene. Twenty shelves were used for each set of MS VIGS experiments

424   within the same time frame. Individual plants were planted in 16-cm pots and placed in the

425   shelves at a distance of 15 cm from each other (Supplemental Figure S1).

426

RNA extraction and cDNA synthesis

RNA was extracted using TRIZOL reagent (GIBCOBRL-Life technologies, MD, USA) and

subsequently treated with 1 μl DNase (10 U/μl) at 37℃ for 30 min. Two micrograms of total

RNA were reverse-transcribed to cDNA by using Superscript III Reverse transcriptase

(Invitrogen, CA, USA). The mixture included 2 μg of total RNA, 0.5mM of dNTP, and 100 ng

of oligo dT or random hexamer and was incubated at 65℃ for 5 min. Thereafter, the mixture was

kept on ice for 1 min, followed by the addition of 5× first-strand buffer, 5mM DTT, 1 μl RNase

inhibitor, 1 μl Superscript III Reverse transcriptase, and incubation at 50℃ for 50 min as well as

at 70℃ for 15 min.

436

Cloning of target insert genes for VIGS

PDS genes for VIGS were searched from GenBank. Fragments were amplified from *N.*

benthamiana PDS (nbpds) and *Cucumis melo* L. *PDS* (cmpds) via RT-qPCR (Accession No.

DQ469932 and KC507802, respectively). Nbpds was amplified by a primer set of Nbpds-F and

Nbpds-R. Cucumber (cspds), melon (cmpds) were amplified by a primer set of cucurbit pds-F

and cucurbit pds-R and watermelon *pds* (ccpds) was amplified by a primer set of ccpds-F and

ccpds-R (Table S2). The *PDS* genes were cloned into pCF93, pCF157, pCF93K, and pCF157K

(Figure 1). Putative male sterility-related genes were deduced from reference-based and *de novo*

RNA-seq in male sterile and fertile watermelon lines previously reported by our group (Rhee et

al., 2015; Rhee et al., 2017). pCF93-pds.int, constructed by inserting a partial fragment of pds

intron into the MCS region of pCF93, was used as a mock. To amplify the intron region of

watermelon pds gene, we isolated the genomic DNA from watermelon cultigen 'Chris cross'

25

449   using DNeasy plant mini kit (Qiagen, CA, USA) followed the manufacturer's manual. The target

450   genes and primer sequences are presented in Table S1 and S2, respectively. The primer sets were

451   designed based on the watermelon 97103 genome v1 at CuGenDB

452   (http://cucurbitgenomics.org/).

453   Total RNA was reverse-transcribed to cDNA by using Superscript III Reverse transcriptase

454   (Invitrogen, CA, USA) and oligo dT. cDNA was then amplified using Phusion DNA polymerase

455   (Thermo, MA, USA). The PCR conditions were as follows: 98℃ for 30 sec, 35 cycles of 98℃

456   for 10 sec, 60℃ for 30 sec, 72℃ for 30 sec, and 72℃ for 2 min. Each *Xho*I-*Pme*I-digested PCR

457   fragment was ligated into the pCF93.

458

459   **Agroinoculation**

460   All constructed vectors were transformed into *Agrobacterium tumefaciens* Gv3101. A single

461   colony was picked up and cultured overnight in 5 ml LB media at 28℃. 100 µl of cultured cell-

462   containing medium was transferred to fresh 30 ml LB medium containing 0.01M MES (pH 5.6)

463   and 20 µM of acetosyringone. The cells were grown to an OD 600 of 1.0 and then harvested via

464   centrifugation. Harvested cells were resuspended with MMA medium to a final O.D 600 of 0.9,

465   and 200 µM acetosyringone was added. The inoculums were incubated at room temperature for 4

466   h with gentle agitation. The cells were inoculated onto cotyledons of cucurbits and *N.*

467   *benthamiana*. Three true leaves per plant were used for inoculation. The agrobacterium solution

468   was injected into the abaxial manner of leaves by using a 1-ml needleless syringe.

469

470   **RT-qPCR**

471   We collected pooled leaf samples from individual *N. benthamiana* and cucurbit plants and

472   isolated total RNA from three individual plants in triplicate in order to analyze VIGS efficiency

473   via RT-qPCR. To determine gene expression levels in flowers, three individual flowers were

474   used for total RNA isolation and cDNA synthesis. One microliter of cDNA was subjected to RT-

475   qPCR. 18S rDNA and glyceraldehyde 3-phosphate dehydrogenase (GAPDH) were used as

476   internal controls in *N. benthamiana* and cucurbits, respectively. RT-qPCR was conducted using

477   Eco Real-Time PCR (Illumina, CA, USA). The PCR mixture included 10 µl 2× Realtime PCR

478   mix (Biofact, Daejeon, Korea), 1 µl Evagreen dye, 10 µM primers, 1 µl cDNA, and ddH$_2$O up to

479   a total volume of 20 µl. PCR conditions were as follows: 95°C for 12 min, 40 cycles of 95°C for

480   10 s, 60°C for 15 s, and 68°C for 15 s. We determined relative gene expression via the ddCT

481   method. For statistical analysis of relative gene expression, one-way ANOVA Dunnett's post hoc

482   test was applied using PRISM 6 software.

483

484   Quantification of chlorophyll contents

485   We collected 0.5 g of watermelon peels (approximately ten discs, 10 mm in diameter) and put

486   them in 30 ml of absolute acetone overnight in the dark. Chlorophyll a and b contents were

487   measured using a spectrophotometer and 1.00 cm quartz cuvettes with absorbance values at 651

488   and 664 nm, respectively. The formulae for calculating chlorophyll contents were as follows

489   (Mackinney, 1941): chlorophyll a = (16.5 × O.D$_{664}$ - 8.3 × O.D$_{651}$) × A; chlorophyll b = (33.5 ×

490   O.D$_{651}$ – 12.5 × O.D$_{664}$) × A; total chlorophyll = (25.5 × O.D$_{651}$ - 4 × O.D$_{664}$) × A (A=Methanol

491   volume (L) × 100πr^2 (Cm) × number of leaf disc). A was calculated as 0.385 (A = (30/1000) ×

492   100 × 3.14 × 0.5^{2}x 10).

493

494 **Quantification of lycopene and β-carotene contents by using high-performance liquid**

495 **chromatography (HPLC)**

496 For sample preparation, 10 g of fresh watermelon flesh was freeze-dried for a week. The freeze-

497 dried sample (~ 0.1 g) was ground and mixed with silica beads (3-5 μm) (1:1, w/w). One

498 milliliter of ethanol containing 0.5 mM BHT was added to the samples and struck with beads for

499 30 s. The bead-containing liquid samples were then transferred to 15-ml tubes, to each of which,

500 3 ml of petrol ether and 8 ml of 20% sodium chloride were gradually added with vortexing. The

501 sample was centrifuged at 3000 rpm for 10 min, and the supernatant was collected. Finally,

502 Na_2SO_4 was added to the supernatant, which was then filtrated via a PTFE filter (13 mm, 0.2

503 μm; Advantec, USA). The pre-treated samples were analyzed through HPLC by using a Waters

504 chromatography system equipped with reverse-phase column liquid (Kinetex 2.6 μm, C18 100a,

505 100 × 460 mm; Phenomenex, USA).

506

507 **Histological analysis and microscopy**

508 To investigate the anther developmental differences between the MS and MF lines, floral buds

509 and mature flowers were collected from both lines. The samples were soaked in 2.5%

510 glutaraldehyde (v/v) for 90 min and washed in 0.1 M phosphate buffer (pH. 7.2). The samples

511 were then soaked in 1% osmic acid (v/v) for 90 min and washed in 0.1 M phosphate buffer (pH.

512 7.2) at 4°C. Subsequently, the fixed samples were dehydrated using an ethanol gradient (40, 60,

513 80, 90, 95, and 100%) and then embedded in Epon-812 resin. Ultrathin cross-sections of 1500

514 nm thickness were prepared using an ultramicrotome (PT-X, RMC, USA) and stained with

515 Periodic acid–Schiff (PAS) stain.

516 # Acknowledgements

Data availability statement

526   All relevant data can be found within this manuscript and its supporting information files.

Conflict of interest

528   The authors declare no competing interests.

Supplemental data

530   Supplemental Figure S1. Greenhouse plot layout to validate VIGS system for cucurbits.

531   Supplemental Figure S2. RT-PCR and sequence analysis of progeny virus from pCF157K-nbpds

532   to confirm the homologous recombination in *N. benthamiana.*

533   Supplemental Figure S3. Male sterile flowers are produced in candidate gene silenced

534   watermelon.

535   Supplemental Table S1. List of 38 de novo-exclusive differentially-expressed genes (DEDEGs)

536   to validate gene function by VIGS.

537   Supplemental Table S2. Primers used for the construction of VIGS vectors.

538   Supplemental Table S3. Primers for RT-qPCR.

References

Antignus Y, Wang Y, Pearlsman M, Lachman O, Lavi N, Gal-On A (2001) Biological and molecular characterization of a new cucurbit-infecting tobamovirus. Phytopathology **91:** 565-571

Bekele D, Tesfaye K, Fikre A (2019) Applications of Virus Induced Gene Silencing (VIGS) in Plant Functional Genomics Studies. Journal of Plant Biochemistry & Physiology **7:** 1-7

Benavente LM, Ding XS, Redinbaugh MG, Nelson R, Balint-Kurti P (2012) Virus-induced gene silencing in diverse maize lines using the Brome mosaic virus-based silencing vector. Maydica **57:** 206-214

Bu R, Wang R, Wei Q, Hu H, Sun H, Song P, Yu Y, Liu Q, Zheng Z, Li T (2019) Silencing of glycerol-3-phosphate acyltransferase 6 (GPAT6) gene using a newly established virus induced gene silencing (VIGS) system in cucumber alleviates autotoxicity mimicked by cinnamic acid (CA). Plant and Soil **438:** 329-346

Burgos-Rivera B, Dawe RK (2012) An Arabidopsis tissue-specific RNAi method for studying genes essential to mitosis. PLoS One **7:** e51388

Chen L, Liu YG (2014) Male sterility and fertility restoration in crops. Annu Rev Plant Biol **65:** 579-606

Coimbra S, Almeida J, Junqueira V, Costa ML, Pereira LG (2007) Arabinogalactan proteins as molecular markers in Arabidopsis thaliana sexual reproduction. Journal of Experimental Botany **58:** 4027-4035

Cosgrove DJ, Bedinger P, Durachko DM (1997) Group I allergens of grass pollen as cell wall-loosening agents. Proc Natl Acad Sci U S A **94:** 6559-6564

Culver JN, Lehto K, Close SM, Hilf ME, Dawson WO (1993) Genomic position affects the expression of tobacco mosaic virus movement and coat protein genes. Proc Natl Acad Sci U S A **90:** 2055-2059

Fister AS, Landherr L, Maximova SN, Guiltinan MJ (2018) Transient Expression of CRISPR/Cas9 Machinery Targeting TcNPR3 Enhances Defense Response in Theobroma cacao. Front Plant Sci **9:** 268

569   **Fu DQ, Zhu BZ, Zhu HL, Jiang WB, Luo YB** (2005) Virus-induced gene silencing in
570   tomato fruit. Plant J **43:** 299-308

571   **Gupta RM, Musunuru K** (2014) Expanding the genetic editing tool kit: ZFNs,
572   TALENs, and CRISPR-Cas9. J Clin Invest **124:** 4154-4161

573   **Hu B, Li D, Liu X, Qi J, Gao D, Zhao S, Huang S, Sun J, Yang L** (2017) Engineering
574   Non-transgenic Gynoecious Cucumber Using an Improved Transformation
575   Protocol and Optimized CRISPR/Cas9 System. Mol Plant **10:** 1575-1578

576   **Huang L, Cao J, Ye W, Liu T, Jiang L, Ye Y** (2008) Transcriptional differences
577   between the male-sterile mutant bcms and wild-type Brassica campestris ssp.
578   chinensis reveal genes related to pollen development. Plant Biol (Stuttg) **10:**
579   342-355

580   **Igarashi A, Yamagata K, Sugai T, Takahashi Y, Sugawara E, Tamura A, Yaegashi**
581   **H, Yamagishi N, Takahashi T, Isogai M, Takahashi H, Yoshikawa N** (2009)
582   Apple latent spherical virus vectors for reliable and effective virus-induced
583   gene silencing among a broad range of plants including tobacco, tomato,
584   Arabidopsis thaliana, cucurbits, and legumes. Virology **386:** 407-416

585   **Jiang J, Yao L, Yu Y, Lv M, Miao Y, Cao J** (2014) PECTATE LYASE-LIKE10 is
586   associated with pollen wall development in Brassica campestris. J Integr Plant
587   Biol **56:** 1095-1105

588   **Kant R, Sharma S, Dasgupta I** (2015) Virus-induced gene silencing (VIGS) for
589   functional genomics in rice using rice tungro bacilliform virus (RTBV) as a
590   vector. *In* Plant Gene Silencing. Springer, pp 201-217

591   **Kim YJ, Zhang D** (2018) Molecular Control of Male Fertility for Crop Hybrid
592   Breeding. Trends Plant Sci **23:** 53-65

593   **Kulikauskas R, McCormick S** (1997) Identification of the tobacco and Arabidopsis
594   homologues of the pollen-expressed LAT59 gene of tomato. Plant Mol Biol
595   **34:** 809-814

596   **Lara-Gonzalez P, Westhorpe FG, Taylor SS** (2012) The spindle assembly checkpoint.
597   Curr Biol **22:** R966-980

598   **Li C, Yamagishi N, Kasajima I, Yoshikawa N** (2019) Virus-induced gene silencing
599   and virus-induced flowering in strawberry (Fragaria x ananassa) using apple
600   latent spherical virus vectors. Hortic Res **6:** 18

601   **Li H, Zhang D, Xie K, Wang Y, Liao Q, Hong Y, Liu Y** (2021) Efficient and high-
602   throughput pseudorecombinant-chimeric Cucumber mosaic virus-based VIGS
603   in maize. Plant Physiol

604   **Li J, Li Y, Deng Y, Chen P, Feng F, Chen W, Zhou X, Wang Y** (2018) A calcium-
605   dependent protein kinase, ZmCPK32, specifically expressed in maize pollen to
606   regulate pollen tube growth. PLoS One **13:** e0195787

607   **Li J, Yu M, Geng LL, Zhao J** (2010) The fasciclin-like arabinogalactan protein gene,
608   FLA3, is involved in microspore development of Arabidopsis. Plant J **64:** 482-
609   497

610   **Liao JJ, Wang CH, Xing QJ, Li YP, Liu XF, Qi HY** (2019) Overexpression and VIGS
611   system for functional gene validation in oriental melon (Cucumis melo var.
612   makuwa Makino). Plant Cell, Tissue and Organ Culture (PCTOC) **137:** 275-284

613   **Lin MK, Belanger H, Lee YJ, Varkonyi-Gasic E, Taoka K, Miura E, Xoconostle-**
614   **Cazares B, Gendler K, Jorgensen RA, Phinney B, Lough TJ, Lucas WJ** (2007)
615   FLOWERING LOCUS T protein may act as the long-distance florigenic signal in
616   the cucurbits. Plant Cell **19:** 1488-1506

617   **Lindbo JA** (2007) TRBO: a high-efficiency tobacco mosaic virus RNA-based
618   overexpression vector. Plant Physiol **145:** 1232-1240

619   **Liu N, Xie K, Jia Q, Zhao J, Chen T, Li H, Wei X, Diao X, Hong Y, Liu Y** (2016)
620   Foxtail Mosaic Virus-Induced Gene Silencing in Monocot Plants. Plant Physiol
621   **171:** 1801-1807

622   **Liu Y, Schiff M, Dinesh-Kumar SP** (2002) Virus-induced gene silencing in tomato.
623   Plant J **31:** 777-786

624   **Lyu M, Liang Y, Yu Y, Ma Z, Song L, Yue X, Cao J** (2015) Identification and
625   expression analysis of BoMF25, a novel polygalacturonase gene involved in
626   pollen development of Brassica oleracea. Plant Reprod **28:** 121-132

627 **Mackinney G** (1941) Absorption of light by chlorophyll solutions. J. Biol. Chem. **140:**
628   315-322

629 **Manzano S, Martinez C, Garcia JM, Megias Z, Jamilena M** (2014) Involvement of
630   ethylene in sex expression and female flower development in watermelon
631   (Citrullus lanatus). Plant Physiol Biochem **85:** 96-104

632 **Mei Y, Zhang C, Kernodle BM, Hill JH, Whitham SA** (2016) A Foxtail mosaic virus
633   Vector for Virus-Induced Gene Silencing in Maize. Plant Physiol **171:** 760-772

634 **Myers C, Romanowsky SM, Barron YD, Garg S, Azuse CL, Curran A, Davis RM,**
635   **Hatton J, Harmon AC, Harper JF** (2009) Calcium-dependent protein kinases
636   regulate polarized tip growth in pollen tubes. Plant J **59:** 528-539

637 **Pennell RI, Roberts K** (1990) Sexual development in the pea is presaged by altered
638   expression of arabinogalactan protein. Nature **344:** 547-549

639 **Pickar-Oliver A, Gersbach CA** (2019) The next generation of CRISPR-Cas
640   technologies and applications. Nat Rev Mol Cell Biol **20:** 490-507

641 **Purkayastha A, Mathur S, Verma V, Sharma S, Dasgupta I** (2010) Virus-induced
642   gene silencing in rice using a vector derived from a DNA virus. Planta **232:**
643   1531-1540

644 **Rhee S-J, Jang YJ, Ko YJ, Lee GP** (2018) Identification of the pleiotropic function of
645   TOUSLED kinase in tomato (Solanum lycopersicum L.) using a Cucumber
646   mosaic virus-based vector. Horticulture, Environment, and Biotechnology **59:**
647   105-114

648 **Rhee SJ, Hong JS, Lee GP** (2014) Infectivity and complete nucleotide sequence of
649   cucumber fruit mottle mosaic virus isolate Cm cDNA. Arch Virol **159:** 1807-
650   1811

651 **Rhee SJ, Jang YJ, Lee GP** (2016) Identification of the subgenomic promoter of the
652   coat protein gene of cucumber fruit mottle mosaic virus and development of
653   a heterologous expression vector. Arch Virol **161:** 1527-1538

654 **Rhee SJ, Kwon T, Seo M, Jang YJ, Sim TY, Cho S, Han SW, Lee GP** (2017) De
655   novo-based transcriptome profiling of male-sterile and fertile watermelon
656   lines. PLoS One **12:** e0187147

657 **Rhee SJ, Seo M, Jang YJ, Cho S, Lee GP** (2015) Transcriptome profiling of
658 differentially expressed genes in floral buds and flowers of male sterile and
659 fertile lines in watermelon. BMC Genomics **16:** 914

660 **Robertson D** (2004) VIGS vectors for gene silencing: many targets, many tools. Annu
661 Rev Plant Biol **55:** 495-519

662 **Senthil-Kumar M, Mysore KS** (2011) Virus-induced gene silencing can persist for
663 more than 2 years and also be transmitted to progeny seedlings in Nicotiana
664 benthamiana and tomato. Plant Biotechnology Journal **9:** 797-806

665 **Shah JV, Cleveland DW** (2000) Waiting for anaphase: Mad2 and the spindle
666 assembly checkpoint. Cell **103:** 997-1000

667 **Shan S, Soltis PS, Soltis DE, Yang B** (2020) Considerations in adapting CRISPR/Cas9
668 in nongenetic model plant systems. Appl Plant Sci **8:** e11314

669 **Shivprasad S, Pogue GP, Lewandowski DJ, Hidalgo J, Donson J, Grill LK, Dawson**
670 **WO** (1999) Heterologous sequences greatly affect foreign gene expression in
671 tobacco mosaic virus-based vectors. Virology **255:** 312-323

672 **Switzenberg JA, Beaudry RM, Grumet R** (2015) Effect of CRC::etr1-1 transgene
673 expression on ethylene production, sex expression, fruit set and fruit ripening
674 in transgenic melon (Cucumis melo L.). Transgenic Res **24:** 497-507

675 **Tian S, Jiang L, Cui X, Zhang J, Guo S, Li M, Zhang H, Ren Y, Gong G, Zong M,**
676 **Liu F, Chen Q, Xu Y** (2018) Engineering herbicide-resistant watermelon variety
677 through CRISPR/Cas9-mediated base-editing. Plant Cell Rep **37:** 1353-1356

678 **Tian S, Jiang L, Gao Q, Zhang J, Zong M, Zhang H, Ren Y, Guo S, Gong G, Liu F,**
679 **Xu Y** (2017) Efficient CRISPR/Cas9-based gene knockout in watermelon. Plant
680 Cell Rep **36:** 399-406

681 **Tomes M, Johnson K, Hess M** (1963) The carotene pigment content of certain red
682 fleshed watermelons. *In* Proc. Am. Soc. Hortic. Sci, **82:** 460-464

683 **Tzean Y, Lee MC, Jan HH, Chiu YS, Tu TC, Hou BH, Chen HM, Chou CN, Yeh HH**
684 (2019) Cucumber mosaic virus-induced gene silencing in banana. Sci Rep **9:**
685 11553

686 **Wang DH, Li F, Duan QH, Han T, Xu ZH, Bai SN** (2010) Ethylene perception is
687   involved in female cucumber flower development. Plant J **61:** 862-872

688 **Wang W, Scali M, Vignani R, Milanesi C, Petersen A, Sari-Gorla M, Cresti M**
689   (2004) Male-sterile mutation alters Zea m 1 (β-expansin 1) accumulation in a
690   maize mutant. Sexual Plant Reproduction **17:** 41-47

691 **Xie W, Marty DM, Xu J, Khatri N, Willie K, Moraes WB, Stewart LR** (2021)
692   Simultaneous gene expression and multi-gene silencing in Zea mays using
693   maize dwarf mosaic virus. BMC Plant Biol **21:** 208

694 **Yamamoto K, Grzech D, Koudounas K, Stander EA, Caputi L, Mimura T,**
695   **Courdavault V, O'Connor SE** (2021) Improved virus-induced gene silencing
696   allows discovery of a serpentine synthase gene in Catharanthus roseus. Plant
697   Physiol **187:** 846-857

698 **Ye J, Xu M** (2012) Actin bundler PLIM2s are involved in the regulation of pollen
699   development and tube growth in Arabidopsis. J Plant Physiol **169:** 516-522

700 **Yu HG, Muszynski MG, Kelly Dawe R** (1999) The maize homologue of the cell cycle
701   checkpoint protein MAD2 reveals kinetochore substructure and contrasting
702   mitotic and meiotic localization patterns. J Cell Biol **145:** 425-435

703 **Yu J, Gao L, Liu W, Song L, Xiao D, Liu T, Hou X, Zhang C** (2019) Transcription
704   Coactivator ANGUSTIFOLIA3 (AN3) Regulates Leafy Head Formation in
705   Chinese Cabbage. Front Plant Sci **10:** 520
706